THE JOURNAL OF BIOLOGICAL CHEMISTRY
Vol. 279, No. 26, Issue of June 25, pp. 27466–27471, 2004

Printed in U.S.A.

Allosteric β_1 Integrin Antibodies That Stabilize the Low Affinity State by Preventing the Swing-out of the Hybrid Domain*

Received for publication, April 20, 2004, and in revised form, April 27, 2004
Published, JBC Papers in Press, April 27, 2004, DOI 10.1074/jbc.M404354200

Bing-Hao Luo‡, Konstantin Strokovich§, Thomas Walz§, Timothy A. Springer‡, and Junichi Takagi¶‖

From the ‡The CBR Institute for Biomedical Research and Department of Pathology and the §Department of Cell Biology, Harvard Medical School, Boston, Massachusetts 02115 and the ¶Institute for Protein Research, Laboratory of Protein Synthesis and Expression, Osaka University, 3-2 Yamadaoka, Suita, Osaka 565-0871, Japan

The ligand binding function of integrins can be modulated by various monoclonal antibodies by both direct and indirect mechanisms. We have characterized an anti-β_1 antibody, SG/19, that had been reported to inhibit the function of the β_1 integrin on the cell surface. SG/19 recognized the wild type β_1 subunit that exists in a conformational equilibrium between the high and low affinity states but bound poorly to a mutant β_1 integrin that had been locked in a high affinity state. Epitope mapping of SG/19 revealed that Thr^{82} in the β_1 subunit, located at the outer face of the boundary between the I-like and hybrid domains, was the key binding determinant for this antibody. Direct visualization of the $\alpha_5\beta_1$ headpiece fragment in complex with SG/19 Fab with electron microscopy confirmed the location of the binding surface and showed that the ligand binding site is not occluded by the bound Fab. Surface plasmon resonance showed that $\alpha_5\beta_1$ integrin bound by SG/19 maintained a low affinity toward its physiological ligand fibronectin (Fn) whereas binding by function-blocking anti-α_5 antibodies resulted in a complete loss of fibronectin binding. Thus a class of the anti-β antibodies represented by SG/19 attenuate the ligand binding function by restricting the conformational shift to the high affinity state involving the swing-out of the hybrid domain without directly interfering with ligand docking.

Integrins are cell adhesion molecules that bind to ligands in the extracellular matrix and on cell surfaces and regulate many biological functions including cell migration. The affinity of integrins for ligands is conformationally regulated (1–4). On physiological cell surfaces, integrins can assume multiple conformations with distinct affinity states, with the low affinity state being predominant. Physiological "inside-out" signals that impinge on integrin cytoplasmic domains and activating or inhibitory mAbs[1] that bind to the integrin extracellular domain are thought to alter the equilibrium between different conformational states. Electron microscopic (EM) studies of the extracellular domain, fluorescence resonance energy transfer and NMR studies on the cytoplasmic domains, and disulfide cross-linking of the transmembrane domains have indicated that close apposition of the membrane-proximal region of each subunit and the overall bent structure are hallmarks for the low affinity state of integrins, whereas the extended conformation with separated legs represents the high affinity state (5–8).

Monoclonal antibodies have been instrumental to studies on the structure and function of integrins (9). Integrin mAbs can be divided into three classes: (i) "inhibitory mAbs" that perturb biological function *i.e.* ligand binding, (ii) "stimulatory mAbs" that augment ligand binding, and (iii) "neutral mAbs" that do not have any impact on activity. Although some inhibitory mAbs directly recognize the ligand binding site on the integrin molecule and act as ligand-mimetic competitive inhibitors, another class of inhibitory mAbs bind outside the ligand binding site and seem to inhibit integrin function allosterically (10, 11). It is assumed that this class of mAbs exert their effect by stabilizing the unoccupied state of the receptor or by preventing a conformational change necessary for ligand occupancy, in a manner opposite from that of stimulating mAbs (12). However, the mechanism by which these mAbs affect the conformational change in integrins has not been determined nor has the effect of these mAbs on the ligand binding kinetics of integrins been investigated. Here we present direct evidence that a class of allosteric anti-β_1 mAbs, represented by SG/19, binds distal to the ligand binding site across the interface between the I-like and hybrid domains of the β_1 subunit and prevents interconversion of the receptor conformation by blocking the hybrid domain swing-out. The restriction imposed by mAb binding maintains the integrin in a low, but not zero, affinity state.

EXPERIMENTAL PROCEDURES

Monoclonal Antibodies—The murine anti-human β_1 mAbs SG/19 (IgG1) and SG/7 (IgA) were kindly provided by Dr. K. Miyake (13). Murine anti-human β_1 mAbs TS2/16 (14), K20 (15), rat anti-human α_5 mAbs 16 (16), 11 (17), and rat anti-human β_1 mAb 13 (16) were obtained from the Fifth International Leukocyte Workshop (18). Murine anti-β_1 mAbs JB1 (19), 12G10 (20), HUTS-4 (21), and α_5 mAb P1D6 (22) were purchased from Chemicon International Inc. (Temecula, CA). The Fab fragment of SG/19 IgG was prepared as described previously (23).

Transfection and mAb Binding—Plasmids coding for full-length wild type or G429N mutant human β_1 were subcloned into pEF1/V5-HisA and introduced into the CHO-K1 cells using calcium phosphate precipitation. After selecting the transfected cells in a medium containing 1 mg/ml Geneticin G418 for 1 week, the surviving cells were sorted by fluorescence-activated cell sorting to obtain cell lines expressing the desired level of human β_1 integrins. For epitope mapping, CHO-K1 cells transfected with a human β_1 chain carrying single point mutation were cultured in a medium containing 1 mg/ml Geneticin G418 for 2 weeks, and the surviving cell population was tested for reactivity against

* This work was supported in part by Grant HL48675 from the National Institutes of Health (to T. A. S. and J. T.) and grants from the Kato Memorial Bioscience Foundation and the Mitsubishi Pharma Research Foundation. The molecular EM facility at Harvard Medical School was established by a generous donation from the Giovanni Armenise Harvard Center for Structural Biology and is maintained by funds from National Institutes of Health Grant GM62580. The costs of publication of this article were defrayed in part by the payment of page charges. This article must therefore be hereby marked "*advertisement*" in accordance with 18 U.S.C. Section 1734 solely to indicate this fact.

‖ To whom correspondence should be addressed. Tel.: 81-6-6879-8607; Fax: 81-6-6879-8609; E-mail: takagi@protein.osaka-u.ac.jp.

[1] The abbreviations used are: mAb, monoclonal antibody; EM, electron microscopic; Fn, fibronectin; SPR, surface plasmon resonance; CHO, Chinese hamster ovary.

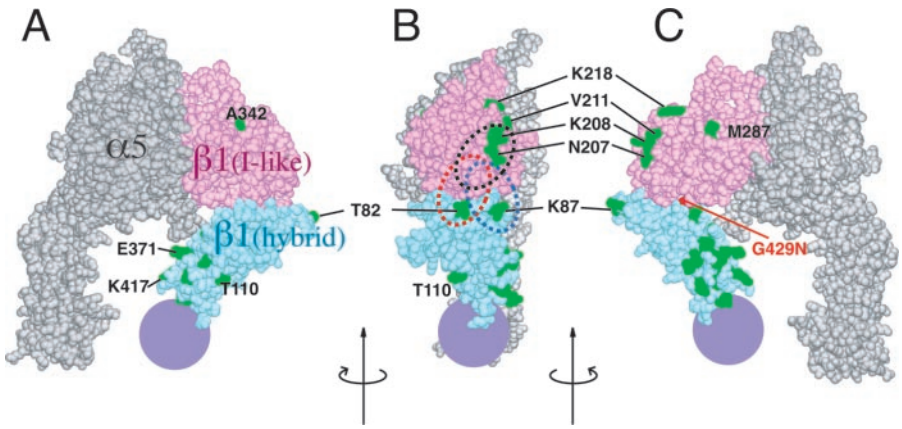

FIG. 1. **Three-dimensional model of the $\alpha_5\beta_1$ integrin headpiece.** A model of the $\alpha_5\beta_1$ headpiece fragment comprising the α_5 β-propeller and the thigh domain (both in *gray*) and the β_1 I-like (*magenta*) and hybrid (*cyan*) domains was built using the closed $\alpha_V\beta_3$ structure (PDB code 1JV2) as a template by SWISS-MODEL (37). The location of the PSI domain, which is not seen in the crystal structure, is shown as a *purple sphere*. *A–C*, CPK presentations viewed from three different directions rotated by 90° about the vertical axis. β_1 residues that differ between human and mouse are painted *green* with key residues labeled. The position of the activating mutation G429N is also labeled in *red*. Putative binding footprints for inhibitory mAbs 13, SG/19, and SG/7 are marked by a *black*, *red*, and *blue dotted oval*, respectively.

various mAbs without further cloning. Bindings of mAbs were evaluated by fluorescence-activated cell sorting analysis using either anti-mouse or anti-rat IgG conjugated with fluorescein isothiocyanate. Fibronectin binding was evaluated by incubating human β_1-expressing cells with 50 μg/ml bovine plasma fibronectin labeled with fluorescein isothiocyanate in the presence or absence of activating mAb TS2/16 (10 μg/ml) at room temperature for 30 min followed by flow cytometric analysis.

Negative Stain EM of $\alpha_5\beta_1$ Head Fragment—A soluble $\alpha_5\beta_1$ headpiece fragment containing α_5 residues 1–623 and β_1 residues 1–445 was produced and purified as described previously (24). The construct contained a disulfide-bonded C-terminal "clasp," which was removed specifically by tobacco etch virus protease treatment prior to the analysis. Unclasped $\alpha_5\beta_1$ fragment was incubated with a saturating concentration of SG/19 Fab fragment or Fn7–10 fragment and purified on a Superdex 200 HR column equilibrated with 50 mM Tris HCl, pH 7.5, 150 mM NaCl, containing 1 mM $MnCl_2$. The peak fraction was adsorbed to glow-discharged carbon-coated copper grids, stained with uranyl formate, and inspected with an FEI Tecnai 12 electron microscope operated at 120 kV. Image processing was performed using the SPIDER image processing package (25) as described previously (24).

Surface Plasmon Resonance (SPR) Binding Assay—Interaction between the recombinant full-length $\alpha_5\beta_1$ and recombinant fibronectin fragment was assessed by SPR analysis with a BIAcore 3000 (Biacore AB) as described previously (26). Briefly, 1.7 μg of $\alpha_5\beta_1$ was incubated with 4.2 μg of purified IgG for >30 min in Tris-buffered saline containing 1 mM $MnCl_2$, diluted to give a final concentration of 20–40 nM, and flowed at 20 μl/min at 25 °C over a streptavidin-coated sensor chip immobilized with biotinylated Fn7–10 at a density of ~500 resonance units. All measurements were base line-corrected by subtracting the sensorgram obtained with a control streptavidin surface, and kinetic parameters were determined by fitting the data to a 1:1 Langmuir binding model using BIAevaluation software version 3.0.

RESULTS

The SG/19 Epitope Maps to Thr^{82} in the Hybrid Domain of the β_1 Subunit—SG/19 was originally identified as a mouse mAb that blocked binding of the Nalm-6 human pre-B cell line to the murine stromal cell line BMS2 (13). It strongly inhibits β_1 integrin-mediated cell adhesion at 10 μg/ml (13). Whereas most function-blocking mAb to β_1 bind to the I-like domain (9, 27), SG/19 maps to a more N-terminal region in the β_1 subunit (28). Within this N-terminal region, only 4 residues in the PSI domain and 7 residues in the hybrid domain differ between human and mouse β_1. Although these domains are not known to be implicated in the ligand binding function, inspection of a homology model of $\alpha_5\beta_1$ reveals that 2 of these 11 species-specific residues (*i.e.* Thr^{82} and Lys^{87}) are positioned very close to the ligand binding I-like domain (Fig. 1) and thus are likely candidates for the SG/19 epitope. These residues were individually mutated to the corresponding murine residue, and the reactivity of SG/19 was evaluated. As shown in Table I, the binding of SG/19 to the β_1 chain was critically dependent on Thr^{82}, whereas the mutation at Lys^{87} did not affect the binding. Conversely, the binding of another function-blocking mAb, SG/7, which had been reported to recognize a Ca^{2+}-dependent epitope (29) was totally abolished by the mutation of Lys^{87} and only partially by the mutation of Thr^{82}. Mutation of species-specific residues in the I-like domain, *i.e.* N207D, K208R, V211F, K218Q, M287V, and A342G, did not affect the binding of either mAb.

Rat anti-human β_1 mAb 13 has been characterized extensively and reported to block human β_1 integrin function by an allosteric mechanism (11). The epitope for mAb 13 had been mapped to residues 207–218 in the β_1 I-like domain (27). Our results revealed that mAb 13 recognizes a combinatorial epitope made by Asn^{207}, Lys^{208}, and Val^{211} with Asn^{207} contributing the most (Table I). Next we explored whether SG/19 and mAb 13 compete with each other for binding to β_1. Cy3-labeled SG/19 was competed out by mAb 13 for binding to wild type human β_1 (Table II). Reciprocally, the binding of mAb 13 was competed by mAb SG/19. Reciprocal competition was also observed between SG/19 and SG/7 mAbs (data not shown) and between mAb SG/7 and mAb 13 (13). In contrast, SG/19 did not compete with two other mAbs, TS2/16 and 4B4, mapped to residues 207–218 (data not shown) indicating that the binding site for mAb 13 is slightly different from that for TS2/16 and 4B4. In the three-dimensional model, Asn^{207}, Thr^{82}, and Lys^{87} are all located in close proximity (Fig. 1*B*). Because the antigen-binding footprints for the three inhibitory mAbs 13, SG/19, and SG/7 are overlapping, they are likely to have similar impacts on the conformation of the junction of the β_1 I-like and hybrid domains to which they bind.

Inhibitory mAbs Show Diminished Binding toward Mutant β_1 Integrin Locked in a High Affinity State—Stimulatory mAbs, upon binding to integrins, shift the conformational equilibrium toward the active conformer. Therefore, stimulatory mAbs generally show increased binding toward activated receptors (9, 23, 30). Allosteric inhibitory mAbs that work in the opposite way are expected to show reduced binding to the active conformer. We have successfully engineered a mutant β_3 integrin constitutively in a high affinity state by introducing an *N*-glycosylation site, *i.e.* a glycan wedge, at the inner side of the bend between the I-like and hybrid domains (31). A previously designed β_1 glycan wedge mutant, β_1-P333N, has a high affin-

TABLE I

Effect of single amino acid substitutions in the N-terminal region of the β_1 chain on the reactivity of anti-β_1 mAbs

CHO-K1 transfectants expressing human β_1 containing the indicated mutations were examined for reactivity with anti-β_1 mAbs by immunofluorescence flow cytometry. 207/208/211 denotes β_1 carrying the combined mutations N207D, K208R, and V211F. The numbers in the table represent the percentages of positive cells in a typical experiment. /+, /±, and /− represent positive, partial, and negative reactivities, respectively.

	Wild type β_1	T82M	K87R	N207D	K208R	V211F	K218Q	M287V	A342G	207/208/211
Control	0.6/−	0.8/−	0.7/−	0.6/−	0.9/−	0.8/−	0.8/−	1.6/−	2.8/−	1.7/−
K20	14.2/+	11.1/+	16.0/+	14.5/+	23.9/+	6.9/+	18.9/+	18.7/+	10.5/+	19.0/+
SG/19	11.7/+	0.6/−	15.8/+	15.6/+	18.1/+	3.9/+	18.1/+	18.1/+	11.4/+	20.7/+
SG/7	12.5/+	4.0/±	0.3/−	13.8/+	15.9/+	4.6/+	17.6/+	15.2/+	7.4/+	13.8/+
13	13.9/+	17.2/+	19.6/+	6.2/±	19.2/+	3.8/+	19.2/+	19.6/+	11.2/+	1.5/−
TS2/16	13.8/+	14.7/+	16.5/+	14.0/+	23.0/+	4.3/+	19.6/+	21.4/+	11.2/+	3.2/−

TABLE II

Competitive binding between mAbs 13 and SG/19

CHO-K1 cells transfected with wild type human β_1 were stained with 5 μg/ml Cy3-labeled mAbs (or unlabeled rat mAb 13 in combination with fluorescein isothiocyanate-anti-rat IgG) in the absence or presence of 50 μg/ml unlabeled antibodies. Binding is expressed as the background-subtracted mean fluorescence intensity as percent of control staining (*i.e.* no unlabeled mAbs). NT, not tested.

Competitor	Binding		
	Cy3-K20	Cy3-SG/19	13
		%	
None	100	100	100
K20	0	108	88
SG/19	93	0.8	14
13	97	2.8	NT

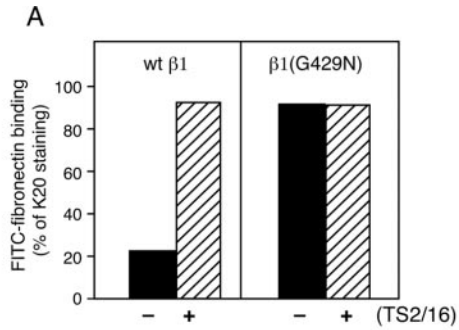

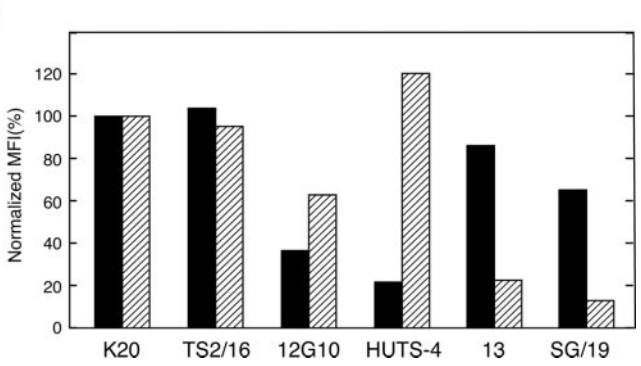

FIG. 2. **Effect of an engineered activating mutation in β_1 on the binding of stimulating and inhibitory mAbs.** *A*, The G429N mutation constitutively activates β_1 integrin. CHO-K1 cells expressing wild type or mutant β_1 integrin were incubated with 50 μg/ml fluorescein isothiocyanate-Fn in the presence (*hatched bar*) or absence (*solid bar*) of 10 μg/ml anti-β_1 activating mAb TS2/16. Ligand bindings are expressed as the mean fluorescence intensities of bound fluorescein isothiocyanate-Fn, after the subtraction of background binding obtained in the presence of 5 mM EDTA, relative to that of non-functional anti-β_1 mAb K20 staining to normalize the differences in the expression level. *B*, CHO-K1 cells expressing wild type (*solid bars*) or G429N mutant (*hatched bars*) β1 integrins were stained with non-functional (K20), stimulatory (TS2/16, 12G10, HUTS-4), or inhibitory (13 and SG/19) β_1 mAbs. The mean fluorescence intensities relative to that of K20 were shown.

ity for ligands (31), although it is less well expressed than wild type and only partially expresses activation epitopes. Therefore, another mutant, β_1-G429N, was designed to introduce an *N*-glycosylation site at Asn^{429} to wedge open the I-like hybrid domain interface (Fig. 1*C*). This mutant shows maximal ligand binding activity in the absence of any activating agents (Fig. 2*A*). This activated β_1 mutant assumes the high affinity conformation in the absence of a bound ligand, as shown by the markedly increased binding of the stimulatory mAbs 12G10 and HUTS-4 compared with binding to the wild type receptor (Fig. 2*B*). Conversely, binding of the inhibitory mAbs 13 and SG/19 was decreased more than 4-fold to the β_1-G429N mutant compared with wild type (Fig. 2*B*). SG/7 also reacted much less well (~70% reduction from wild type) to the wedge mutant (data not shown). A reduction of mAb 13 binding and augmentation of mAb HUTS-4 by an activating mutation in the β_1 I-like domain α7-helix has been reported (32). These effects of the L358A mutation are much less pronounced (~50% reduction and ~50% increase in binding of mAbs 13 and HUTS-4, respectively) than the G429N mutation. As Gly^{429} is located far from the SG/19 epitope at Thr^{82} and the mAb 13 epitope at Asn^{207} (Fig. 1), it is unlikely that mutation of Gly^{429} directly affects binding to these epitopes. Taken together, the data suggest strongly that the inhibitory mAbs 13 and SG/19 prefer the resting (*i.e.* low affinity) conformer and stabilize this conformation upon binding thereby allosterically modulating the ligand binding activity of β_1 integrin.

EM Images of SG/19 Fab Bound to the $\alpha_5\beta_1$ Integrin Headpiece—We next sought to clarify how SG/19 could stabilize a particular conformation of an integrin. In a recent study (24), we utilized negative stain EM and image analysis to visualize a headpiece fragment of $\alpha_5\beta_1$ integrin in the absence and presence of a bound ligand. In the absence of a bound ligand, the $\alpha_5\beta_1$ headpiece assumes the "closed" conformation with the β_1 hybrid domain close to the α subunit (Fig. 3*A* and Ref. 24). Binding to a fragment of the ligand fibronectin changes the conformation dramatically, with an outward swing of the hybrid domain away from the β subunit to assume the "open" conformation (Fig. 3*B* and Ref. 24). The complex of the $\alpha_5\beta_1$ headpiece and SG/19 Fab reveals a clear density for the Fab bound to the side of the β_1 subunit (Fig. 3*C*). The Fab fragment can be easily distinguished by its typical oval shape with a "dimple" corresponding to the thin central part between the V_L/V_H and C_L/C_{H1} lobes. The very uniform orientation of SG/19 Fab relative to the rest of the particle makes it possible to define the binding surface. The antigen binding site of the SG/19 Fab docks to the boundary between the I-like and hybrid domains of the β_1 subunit at the "side" away from the α_5 subunit. This is in perfect agreement with the result of the epitope mapping (see Fig. 1). Importantly, the ligand binding interface located on the top of the receptor is completely exposed and not occluded by the bound Fab (Fig. 3, compare *B*

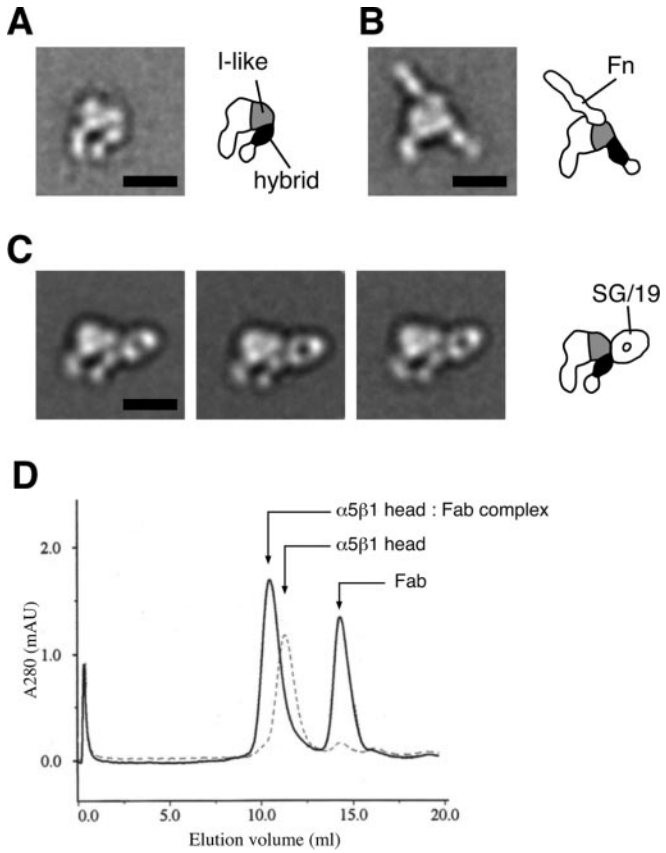

FIG. 3. **Visualization of the $\alpha_5\beta_1$ headpiece fragment in complex with SG/19 Fab.** Projection averages for $\alpha_5\beta_1$ headpiece fragment alone (*A*), in complex with the Fn7–10 fragment (*B*), or in complex with SG/19 Fab (*C*) obtained by negative stain EM are shown. The most (*A* and *B*) or three most (*C*) typical averages are shown, each containing 200–500 particles. *Scale bars*, 100 Å. In the *far right* of each panel, schematic diagrams for the domain organization are also shown. *D*, saturation of SG/19 Fab binding to the $\alpha_5\beta_1$ head fragment. 5.4 μg of $\alpha_5\beta_1$ head fragment was incubated with (*solid line*) or without (*dotted line*) a 2-fold molar excess concentration of SG/19 Fab for 10 min at room temperature and subjected to gel filtration on Superdex 200 at a flow rate of 0.5 ml/min. The elution positions for the $\alpha_5\beta_1$ fragment and its complex with Fab correspond to apparent molecular masses of 190 and 250 kDa, respectively.

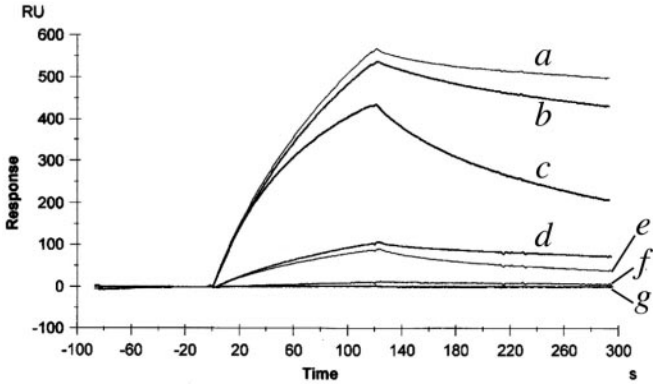

FIG. 4. **Surface plasmon resonance binding analysis of recombinant $\alpha_5\beta_1$ to Fn7–10.** Biotinylated Fn7–10 (~500 resonance units) was immobilized onto a streptavidin-coated chip. Complexes between full-length recombinant $\alpha_5\beta_1$ and mAbs prepared as described under "Experimental Procedures" were injected in a running buffer containing 1 mM Mn^{2+} over the surface for 120 s, and the dissociation phase was followed for 180 s. Antibodies used are *a*, JB1 (anti-β_1, non-functional); *b*, 11 (anti-α_5, non-functional); *c*, no mAb; *d*, 13 (anti-β_1, inhibitory); *e*, SG/19 (anti-β_1, inhibitory); *f*, P1D6 (anti-α_5, inhibitory); and *g*, 16 (anti-α_5, inhibitory). The concentration of the analytes was 20 nM, and the free mAb concentration (in Fab equivalent) during the injection was 140 nM.

TABLE III
Kinetic parameters for $\alpha_5\beta_1$ binding to Fn7–10 fragment

Surface plasmon resonance binding was performed as described under "Experimental Procedures" and the kinetic parameters were derived using the BIAsimulation software. Values are mean ± S.E. obtained from three different analyte concentrations.

Bound mAb	k_{on}	k_{off}	K_D
	$\times 10^5\ M^{-1}\ s^{-1}$	$\times 10^{-3}\ s^{-1}$	nM
None	4.5 ± 0.2	5.5 ± 0.3	12
11	4.5 ± 0.4	2.3 ± 0.3	5.1
SG/19	0.6 ± 0.1	8.9 ± 0.1	151

with *C*). The images show that the binding site of SG/19 centers on the junction between the I-like and hybrid domains, very close to the location of the key antigenic residue Thr^{82}, which is at the domain boundary (see Fig. 1). The binding site of SG/19 clearly includes significant portions of both the I-like and hybrid domains (Fig. 3*C*). This binding site is significantly rearranged when the hybrid domain swings out ~70° upon binding fibronectin (Fig. 3*B*) so that it is unlikely that SG/19 could bind to it. These findings suggest that SG/19 prevents the outward swing of the hybrid domain, trapping the integrin in a low affinity conformation.

$\alpha_5\beta_1$ Bound by Inhibitory Anti-β_1 mAbs Has Low but Detectable Affinity for Ligands—The ligand binding characteristics of $\alpha_5\beta_1$ integrin bound by inhibitory mAbs was measured using SPR to determine whether these mAbs abolished ligand binding, or maintained $\alpha_5\beta_1$ in a low affinity state. To ensure saturation, purified recombinant $\alpha_5\beta_1$ integrin was preincubated with purified mAbs in large excess. Incubation with 1.8 μM SG/19 Fab for 10 min resulted in saturation binding of the $\alpha_5\beta_1$ headpiece with no dissociation detected during ~20 min of gel filtration (Fig. 3*D*). Saturation was also observed with 100 nM SG/19 Fab (not shown). Reaction mixtures containing 140 nM $\alpha_5\beta_1$ headpiece and 560 nM mAb (*i.e.* 1120 nM of Fab equivalents) were diluted up to 7-fold (thus maintaining the concentration of uncomplexed Fab equivalents at >140 nM) and directly infused onto sensor chips coated with fibronectin fragment in a buffer containing 1 mM Mn^{2+}. $\alpha_5\beta_1$ complexed with the non-blocking, non-activating α_5 mAb 11 showed an elevated signal compared with the uncomplexed $\alpha_5\beta_1$ because of the increased mass of the analyte (Fig. 4, compare tracing *b* with *c*). Although mAb 11 binding slightly changed the binding kinetics by decreasing the dissociation rate, this seems to be a general effect of mAb binding, because another non-blocking, non-activating β_1 mAb JB1 (Fig. 4*a*) and an anti-coiled coil tag mAb 2H11(not shown) had a similar effect. The inhibitory α_5 mAbs 16 (Fig. 4*g*) and P1D6 (Fig. 4*f*) completely abolished the binding of $\alpha_{5\beta1}$ headpiece to fibronectin. In contrast, $\alpha_5\beta_1$ complexed with mAb 13 (Fig. 4*d*) or SG/19 (Fig. 4*e*) showed decreased but significant binding to the ligand. Increasing the mAb concentration 2-fold did not alter the binding (not shown). Together with the saturation binding experiments described above, the known K_D of 0.34 nM of mAb 13 for $\alpha_5\beta_1$ (11), and the high concentrations of mAb used in SPR, these results demonstrate that the incomplete inhibition is not because of incomplete saturation of the binding sites by mAbs. Therefore, mAbs SG/19 and 13 decrease the affinity of $\alpha_5\beta_1$ for fibronectin. The kinetic constants (Table III) show that SG/19 binding affected both association and dissociation rate constants resulting in an overall 30-fold drop in the K_D value.

DISCUSSION

Through EM visualization and binding kinetic measurements, we present evidence that anti-β_1 inhibitory mAb SG/19 exerts its effect allosterically. The inhibitory mAbs 13 and SG/7

show similar binding and inhibition characteristics and have an overlapping binding footprint, suggesting that the allosteric mode of inhibition is shared among these three mAbs. In fact, mAb 13 has been reported to be an allosteric inhibitor for ligand binding by $\alpha_5\beta_1$ (11). This notion was based on the fact that mAb 13 binding to β_1 was attenuated by ligand, and the concentration of ligand required for half-maximal inhibition was independent of the mAb concentration. Not only occupation by ligand but also mutations that lock the β_1 integrin in a high affinity state perturb mAb 13 binding (Fig. 2*B* and Ref. 32), supporting the indirect mode of inhibition by this class of mAbs. EM images of the integrin-SG/19 Fab complex clearly show that the mAb docks at the outer hinge connecting the I-like domain and the hybrid domain. This would prevent the outward swing of the hybrid domain and fix the closed conformation of the headpiece that represents the low affinity state (5). Recently, we (33) and others (32) have reported that shape shifting in the α7 helix region of the β I-like domain upregulates ligand affinity. In the context of the whole molecule, this shape shifting causes an outward swing of the β hybrid domain (3, 5, 26). Thus inhibitory mAbs represented by mAb 13 and SG/19 exert their effect by disabling the conformational transition of β I-like domain to the high affinity state. This is exactly the reverse of the mechanism by which the glycan-wedge mutation activates integrins (31). It is not clear whether all anti-β_1 inhibitory mAbs work with a similar indirect mechanism. The inhibitory mAb 4B4 maps to Lys^{218} of the β_1 I-like domain and does not compete with mAb 13, SG/19, or SG/7.[2] The Lys^{218} epitope of 4B4 is more proximal to the ligand binding site (Fig. 1). However, because 4B4 binding is also diminished in the β_1 wedge mutant (data not shown), it is likely that inhibition by 4B4 is, at least in part, allosteric in nature.

Is the allosteric mode specific to β_1 mAb or shared with inhibitory mAb to other integrin β subunits? Inhibitory mAbs to human β_2 are divided into two classes based on the epitope location, one has been mapped to the top of the I-like domain primarily recognizing Glu^{175} or Arg^{122} and the other recognizes a combinatorial epitope involving the side chains of Lys^{133}, His^{322}, and Tyr^{339} (34). Homology modeling of the β_2 I-like domain reveals that the latter residues are situated on the side/bottom face of the I-like domain in a location similar to the epitope residues for mAb 13, SG/19, or SG/7, suggesting the latter class of mAbs to inhibit β_2 integrin function in a way similar to the mAbs described in this paper. All of the anti-β_3 inhibitory mAbs in which the epitopes have been mapped in detail to date recognize the top part of the I-like domain (35), and it is not known whether these mAbs inhibit β_3 integrin function directly or indirectly. Inspection of the β_3 integrin structure reveals that human/mouse species-specific residues are excluded from the outer hinge region between the I-like and hybrid domains, suggesting that mouse anti-human allosteric inhibitory mAbs against β_3 similar to SG/19 could not be obtained because of the sequence conservation.

Mould *et al.* (10) have reported that anti-α_5 mAbs also primarily work as allosteric inhibitors. This notion was again based on the fact that the binding of inhibitory anti-α_5 mAbs were non-competitively attenuated by the bound ligand. However, our SPR experiments clearly showed that $\alpha_5\beta_1$ bound by anti-α_5 mAb 16 or P1D6 had no detectable affinity for ligand, in contrast to the decreased but significant ligand affinity of the SG/19-bound form (Fig. 4). This strongly suggests that the mechanisms for the inhibition are quite different between these two classes of mAbs. EM imaging of the complex of Fn7–10 with the $\alpha_5\beta_1$ headpiece fragment revealed that the 10th module docked onto the α/β interface with the 7–9th modules located close to the α_5 subunit, although a direct interaction between the 9th module and the α_5 β-propeller domain was not evident (Fig. 3*B* and Ref. 24). It is therefore possible that binding of anti-α_5 mAbs to the top of the α_5 β-propeller sterically precludes the approach of the Fn7–9 portion, even if the binding site is distinct from the ligand binding pocket.

The present study underscores the strength of EM imaging in analyzing the conformation of protein complexes. The determination of epitope residues by mutagenesis, combined with three-dimensional structure information, generally leads to a reasonable assumption about the binding mode of an antibody. Direct visualization of the antigen-antibody complex, however, reveals not only the location of the actual interface but also elucidates the impact of antibody binding on the conformation of the target protein. In contrast to x-ray crystal structures, which usually show one of several possible low energy conformations, molecular EM samples the entire set of conformations of single particles and can thus produce structures for all of the major conformations present in the protein population. Another advantage is that EM imaging can be accomplished with a relatively small amount of dilute sample.

In conclusion, we have shown that one class of allosteric anti-β_1 mAbs blocks ligand binding by preventing the "swing-out" of the hybrid domain from the I-like domain, thus stabilizing the closed conformation of the integrin headpiece. There may exist another class of allosterically inhibitory mAbs that stabilize the "bent" conformation of integrins by stabilizing the head-tail or α-tail-β-tail interactions. The use of mAbs as a probe for integrin structure and function has yielded a profound understanding of the mechanisms underlying ligand recognition and affinity regulation of integrins. The unique mode of functional perturbation by anti-β_1 integrin mAbs described here may have important implications in developing anti-integrin pharmaceuticals. For example, an antibody that stabilizes the low affinity conformation of an integrin without completely eliminating its function may prove desirable to prevent the oversuppression of integrin activity. Stabilizing the natural low affinity conformation may also be advantageous, because an antagonist-induced conformational change has been implicated in the development of autoantibodies in patients receiving anti-integrin drugs (36).

Acknowledgments—We thank K. Miyake for the SG/19 hybridoma. We thank D. P. DeBottis and N. Magassa for technical assistance.

REFERENCES

1. Hynes, R. O. (2002) *Cell* **110,** 673–687
2. Liddington, R. C., and Ginsberg, M. H. (2002) *J. Cell Biol.* **158,** 833–839
3. Carman, C. V., and Springer, T. A. (2003) *Curr. Opin. Cell Biol.* **15,** 547–556
4. Takagi, J., and Springer, T. A. (2002) *Immunol. Rev.* **186,** 141–163
5. Takagi, J., Petre, B. M., Walz, T., and Springer, T. A. (2002) *Cell* **110,** 599–611
6. Kim, M., Carman, C. V., and Springer, T. A. (2003) *Science* **301,** 1720–1725
7. Vinogradova, O., Velyvis, A., Velyviene, A., Hu, B., Haas, T. A., Plow, E. F., and Qin, J. (2002) *Cell* **110,** 587–597
8. Luo, B.-H., Springer, T. A., and Takagi, J. (2004) *PLoS Biol.* in press
9. Humphries, M. J. (2000) *Biochem. Soc. Trans.* **28,** 311–339
10. Mould, A. P., Askari, J. A., Aota, S., Yamada, K. M., Irie, A., Takada, Y., Mardon, H. J., and Humphries, M. J. (1997) *J. Biol. Chem.* **272,** 17283–17292
11. Mould, A. P., Akiyama, S. K., and Humphries, M. J. (1996) *J. Biol. Chem.* **271,** 20365–20374
12. Mould, A. P. (1996) *J. Cell Sci.* **109,** 2613–2618
13. Miyake, K., Hasunuma, Y., Yagita, H., and Kimoto, M. (1992) *J. Cell Biol.* **119,** 653–662
14. Hemler, M. E., Sanchez-Madrid, F., Flotte, T. J., Krensky, A. M., Burakoff, S. J., Bhan, A. K., Springer, T. A., and Strominger, J. L. (1984) *J. Immunol.* **132,** 3011–3018
15. Groux, H., Huet, S., Valentin, H., Pham, D., and Bernard, A. (1989) *Nature* **339,** 152–154
16. Akiyama, S. K., Yamada, S. S., Chen, W. T., and Yamada, K. M. (1989) *J. Cell Biol.* **109,** 863–875
17. LaFlamme, S. E., Akiyama, S. K., and Yamada, K. M. (1992) *J. Cell Biol.* **117,** 437–447

[2] J. Takagi, unpublished result.

18. Petruzzelli, L., Luk, J., and Springer, T. A. (1995) in *Leucocyte Typing V: White Cell Differentiation Antigens* (Schlossman, S. F., Boumsell, L., Gilks, W., Harlan, J., Kishimoto, T., Morimoto, T., Ritz, J., Shaw, S., Silverstein, R., Springer, T., Tedder, T., and Todd, R., eds) pp. 1581–1585, Oxford University Press, New York
19. Caixia, S., Stewart, S., Wayner, E., Carter, W., and Wilkins, J. (1991) *Cell. Immunol.* **138,** 216–228
20. Mould, A. P., Garratt, A. N., Askari, J. A., Akiyama, S. K., and Humphries, M. J. (1995) *FEBS Lett.* **363,** 118–122
21. Luque, A., Gomez, M., Puzon, W., Takada, Y., Sanchez-Madrid, F., and Cabanas, C. (1996) *J. Biol. Chem.* **271,** 11067–11075
22. Wayner, E. A., Carter, W. G., Piotrowicz, R. S., and Kunicki, T. J. (1988) *J. Cell Biol.* **107,** 1881–1891
23. Tsuchida, J., Ueki, S., Takada, Y., Saito, Y., and Takagi, J. (1998) *J. Cell Sci.* **111,** 1759–1766
24. Takagi, J., Strokovich, K., Springer, T. A., and Walz, T. (2003) *EMBO J.* **22,** 4607–4615
25. Frank, J., Radermacher, M., Penczek, P., Zhu, J., Li, Y., Ladjadj, M., and Leith, A. (1996) *J. Struct. Biol.* **116,** 190–199
26. Takagi, J., Erickson, H. P., and Springer, T. A. (2001) *Nat. Struct. Biol.* **8,** 412–416
27. Takada, Y., and Puzon, W. (1993) *J. Biol. Chem.* **268,** 17597–17601
28. Mould, A. P., Garratt, A. N., Puzon-McLaughlin, W., Takada, Y., and Humphries, M. J. (1998) *Biochem. J.* **331,** 821–828
29. Miyake, K., Yamashita, Y., and Kimoto, M. (1994) *Int. Immunol.* **6,** 1221–1226
30. Lu, C., Ferzly, M., Takagi, J., and Springer, T. A. (2001) *J. Immunol.* **166,** 5629–5637
31. Luo, B.-H., Springer, T. A., and Takagi, J. (2003) *Proc. Natl. Acad. Sci. U. S. A.* **100,** 2403–2408
32. Mould, A. P., Barton, S. J., Askari, J. A., McEwan, P. A., Buckley, P. A., Craig, S. E., and Humphries, M. J. (2003) *J. Biol. Chem.* **278,** 17028–17035
33. Luo, B.-H., Takagi, J., and Springer, T. A. (2004) *J. Biol. Chem.* **279,** 10215–10221
34. Huang, C., Zang, Q., Takagi, J., and Springer, T. A. (2000) *J. Biol. Chem.* **275,** 21514–21524
35. Puzon-McLaughlin, W., Kamata, T., and Takada, Y. (2000) *J. Biol. Chem.* **275,** 7795–7802
36. Billheimer, J. T., Dicker, I. B., Wynn, R., Bradley, J. D., Cromley, D. A., Godonis, H. E., Grimminger, L. C., He, B., Kieras, C. J., Pedicord, D. L., Spitz, S. M., Thomas, B. E., Zolotarjova, N. I., Gorko, M. A., Hollis, G. F., Daly, R. N., Stern, A. M., and Seiffert, D. (2002) *Blood* **99,** 1–7
37. Peitsch, M. C. (1996) *Biochem. Soc. Trans.* **24,** 274–279